Bunches of misfit dislocations on the onset of relaxation of $Si_{0.4}Ge_{0.6}$/Si(001) epitaxial films revealed by high-resolution x-ray diffraction

Vladimir Kaganer,[1] Tatjana Ulyanenkova,[2] Andrei Benediktovitch,[3] Maksym Myronov,[4] and Alex Ulyanenkov[5]
[1]*Paul-Drude-Institut für Festkörperelektronik, Hausvogteiplatz 5–7, 10117 Berlin, Germany*
[2]*Rigaku Europe SE, Am Hardwald 11, 76275 Ettlingen, Germany*
[3]*Atomicus OOO, Mogilevskaya Str. 39a-530, 220007 Minsk, Belarus*
[4]*The University of Warwick, Department of Physics, Coventry CV4 7AL, United Kingdom*
[5]*Atomicus GmbH, Schoemperlen Str. 12a, 76185 Karlsruhe, Germany*

(Received 14 June 2017; accepted 26 August 2017; published online 12 September 2017)

The experimental x-ray diffraction patterns of a $Si_{0.4}Ge_{0.6}$/Si(001) epitaxial film with a low density of misfit dislocations are modeled by the Monte Carlo method. It is shown that an inhomogeneous distribution of 60° dislocations with dislocations arranged in bunches is needed to explain the experiment correctly. As a result of the dislocation bunching, the positions of the x-ray diffraction peaks do not correspond to the average dislocation density but reveal less than a half of the actual relaxation. *Published by AIP Publishing.* [http://dx.doi.org/10.1063/1.4990135]

I. INTRODUCTION

$Si_{1-x}Ge_x$ films on a Si substrate constitute a heteroepitaxial system that finds numerous applications in the whole compositional range[1] and, at the same time, is a model system that demonstrates the whole spectrum of strain relaxation mechanisms. When either the thickness or the Ge content is small, the layers stay strained, by accepting the lateral lattice spacing of the substrate and expanding vertically due to the Poisson effect. Larger strain is relaxed by one of the two mechanisms: plastic relaxation in planar layers by the introduction of misfit dislocations at the interface[2–5] or development of three-dimensional islands in the Stranski–Krastanov growth mode.[6] Planar films with a controlled strain state are required for various applications. Particularly, the high compressive strain in the $Si_{0.4}Ge_{0.6}$ films, studied in the present work, ought to enhance a room-temperature two-dimensional hole gas mobility, which is important for the application of such films in the field effect transistors.[7]

X-ray diffraction is a well-established technique to characterize relaxed epitaxial films. Positions of the x-ray peaks provide the lattice parameters of a relaxed film and hence the density of misfit dislocations.[8–10] An application of the same analysis at the onset of relaxation suffers from the peak broadening due to a small layer thickness.[11] Moreover, we show below that the inhomogeneity in the dislocation distribution plays an essential role in the x-ray diffraction analysis. The position of the coherent peak is given by the less strained regions of the film and hence underestimates the relaxation. The diffuse x-ray intensity is more sensitive to both the presence of misfit dislocations and their distribution.

II. EXPERIMENTAL

We have chosen for a detailed x-ray diffraction study a 27 nm thick $Si_{0.4}Ge_{0.6}$ film on Si(001), demonstrating an early stage of the relaxation. Thinner unrelaxed and thicker relaxed films of the same series of samples were studied previouly.[12] The samples were grown by reduced pressure chemical vapor deposition in an industrial ASM Epsilon 2000 system. Germane and disilane precursors were used to grow $Si_{0.4}Ge_{0.6}$ epilayers at the growth temperature of 450 °C. The critical thickness for plastic relaxation at a Ge content $x = 0.6$ is 10 nm.[11,13,14] The low growth temperature allows us to obtain 2.7 times thicker layer possessing a small relaxation.

High-resolution x-ray diffraction measurements were performed using a 9 kV SmartLab Rigaku diffractometer with a rotating anode. The diffraction setup included a two-crystal Ge monochromator in the 400 setting and a one-dimensional high-speed position-sensitive detector D/teX Ultra from Rigaku.

III. RESULTS

A. Reciprocal space maps

Figures 1(a)–1(d) present experimental reciprocal space maps in the symmetric 004 and several asymmetric reflections, in a sequence of increasing asymmetry. The wave vectors are represented in the dimensionless units of the product of the components of the reciprocal space vector (q_x, q_z) and the film thickness $d = 27$ nm. Each map comprises a coherent scattering streak extended along the surface normal and diffuse scattering. The presence of the coherent and the diffuse intensities is an indication of a weakly distorted film possessing a low density of misfit dislocations. A closer inspection of the symmetric 004 map in Fig. 1(a) reveals that the positions of the coherent and the diffuse maxima do not coincide: with the origin $q_z = 0$ chosen at the position of the coherent peak, the diffuse intensity is maximum at $q_z d \approx 5.5$.

Figure 2(a) shows line scans extracted from the maps perpendicular to the scattering vectors (ω-scans) at the intensity maxima of the respective maps. For the 004 reflection, two scans are presented: one through the maximum of the coherent intensity (gray line) and the other through the

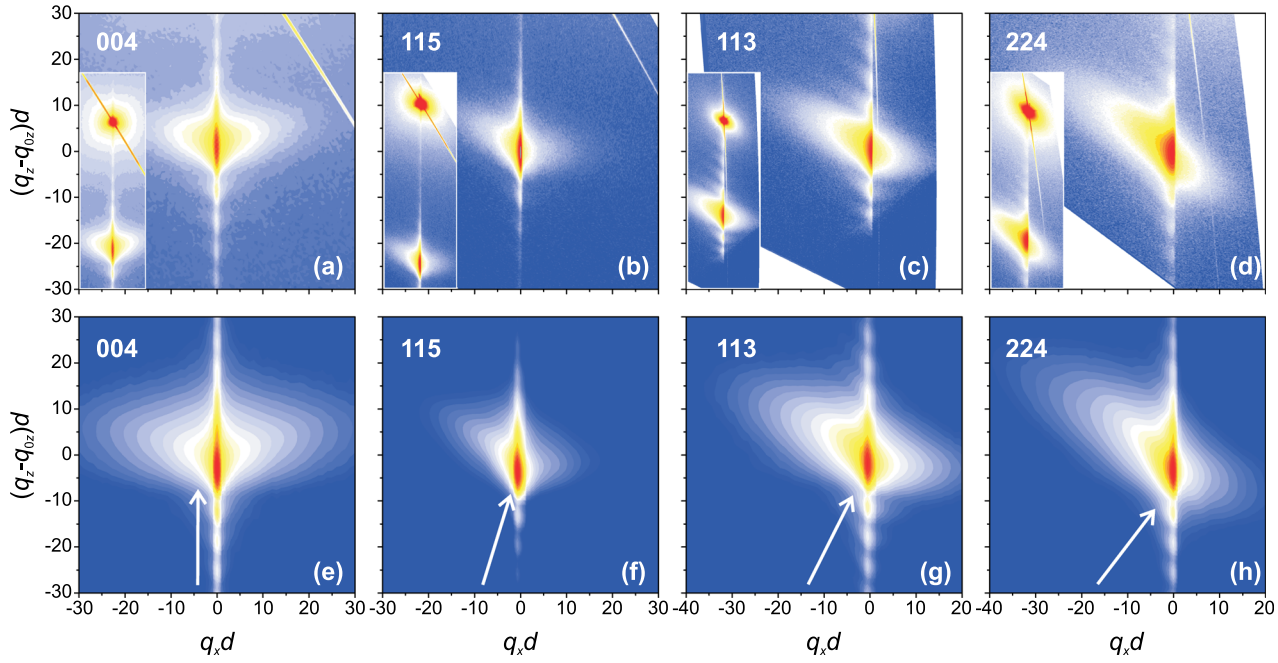

FIG. 1. Experimental [(a)–(d)] and Monte Carlo simulated [(e)–(h)] reciprocal space maps of a 27 nm thick $Si_{0.4}Ge_{0.6}$ film on Si(001). The directions of the scattering vectors are shown by white arrows. The insets in [(a)–(d)] show full reciprocal space maps comprising the substrate and the film peaks.

maximum of the diffuse intensity (green line). Evidently, the former scan shows a larger peak intensity, while the latter has a higher diffuse scattering intensity. In asymmetric reflections, the scans through the coherent and the diffuse maxima reveal a less pronounced (albeit present) difference, and we present only the scans through the coherent maxima.

The reciprocal space maps in asymmetric reflections in Figs. 1(b)–1(d) reveal a strong asymmetry of the diffuse intensity distributions. For each reflection, the coherent streak at $q_x = 0$ separates the diffuse intensity in two lobes: the one at $q_x < 0$ possessing notably higher intensity in comparison to the other at $q_x > 0$. This asymmetry and a sharp border between the two lobes are clearly seen in the scans presented in Fig. 2(a).

Our aim now is to find a distribution of misfit dislocations which complies with all characteristic features of the experimental diffraction patterns in Figs. 1 and 2. The 60° dislocations with Burgers vectors $\frac{1}{2}\langle 011\rangle$ that glide in the $\{111\}$ planes are the main type of dislocations in crystals with diamond or zinc blende structures.[2–5] Calculated and experimental diffraction curves from uncorrelated 60° dislocations show characteristic side peaks (side lobes on the maps)[15–18] that are absent in our experimental patterns. Since edge (Lomer type) misfit dislocations are also formed at the SiGe/Si interface as a result of a reaction between 60° dislocations,[19–21] we have tried various models for the arrangement of edge dislocations, using the Monte Carlo method.[22] However, the calculated profiles are notably narrower than our experimental profiles.

A Monte Carlo method for the calculation of the x-ray diffraction intensity from relaxed epitaxial films has been formulated in Ref. 22. The method is applicable to any kind of misfit dislocations but used so far only for edge (Lomer type) dislocations in symmetric Bragg reflections. The positional correlations of dislocations were considered, implying that the dislocations tend from random to more regular arrangements to reduce the elastic energy of the film. In the present work, we have included 60° dislocations and asymmetric reflections and searched in a wider range of possible positional correlations.

Reciprocal space maps calculated by the Monte Carlo method in Figs. 1(e)–1(h) and the diffraction profiles shown by black lines in Fig. 2 demonstrate a quantitative agreement with the experimental maps and curves. Now, we describe the Monte Carlo model of the dislocation distribution that we have used. We assume two arrays of straight misfit dislocations with the dislocation lines in the two orthogonal $\langle 110\rangle$ directions. For dislocations with the lines normal to the scattering plane (x, z), Burgers vectors $\mathbf{b} = \frac{1}{2}\langle 011\rangle$ have the same component $b_x = -a/2\sqrt{2}$ releasing the misfit, while the signs of two other components, screw $b_y = \pm a/2\sqrt{2}$ and edge $b_z = \pm a/2$, are chosen at random and uncorrelated (here, a is the lattice parameter of the substrate). The position of the Bragg peak corresponding to the average relaxation is given by $q_{0x} = \rho Q_x b_x$ and $q_{0z} = -\frac{2\nu}{1-\nu}\rho Q_z b_x$, where ρ is the linear density of misfit dislocations and Q_x, Q_z are the components of the reciprocal lattice vector.[16] The shift q_{0z} is taken into account in Figs. 1(e)–1(h), but the q_{0x}-shift is not made, as discussed below.

To achieve an agreement between the experimental and the calculated curves in Figs. 1 and 2, we varied the dislocation density and the distribution of dislocations. The dislocation density $\rho d = 0.5$ used in the Monte Carlo calculations corresponds to a relaxation degree $R = 0.05$. The positions of the dislocations are modeled as a Markov chain, with the probability P to have a distance $\rho^{-1}P$ between two subsequent dislocations possessing a lognormal distribution. The probability density is generated as $P = \exp[\mu + \sigma N(0,1)]$, where $N(0, 1)$ is the standard normal distribution with mean 0 and dispersion 1. The standard deviation of the lognormal

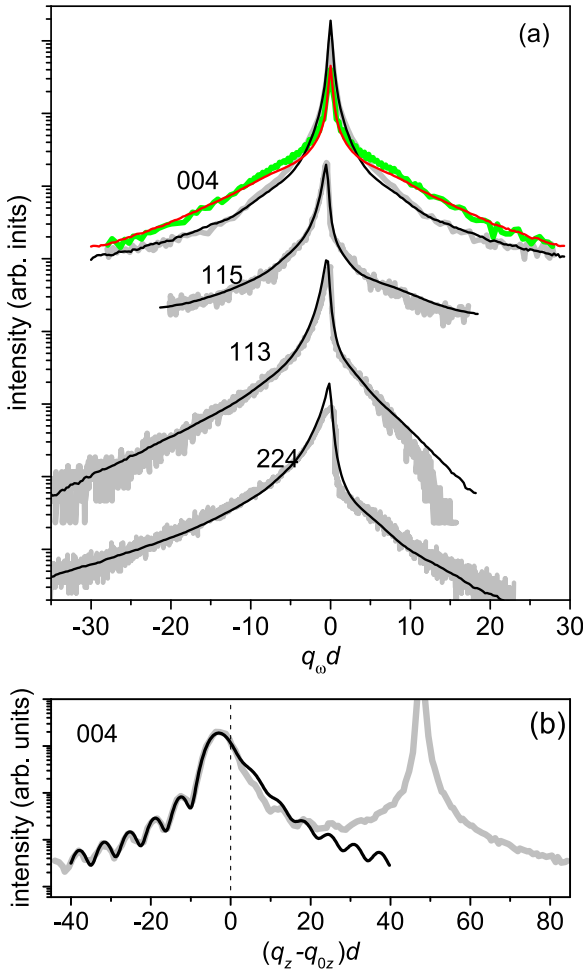

FIG. 2. Scans (a) perpendicular to the diffraction vectors (ω-scans) and (b) along the diffraction vector 004 ($\omega - 2\theta$ scan). The experimental scans are shown by thick gray lines and the Monte Carlo calculated ones by black lines. For 004 reflection, two q_x-scans are plotted. The scan at the position of the coherent maximum on the map in Fig. 1(a) is shown by the gray line, while the scan at the maximum of diffuse scattering is shown by the green line.

distribution is taken to be $s = 10$ times larger than its mean value. Explicitly, the parameters of the lognormal distribution are $\sigma = \sqrt{\ln(1+s^2)} = 2.15$ and $\mu = -\sigma^2/2 = -2.31$.

B. Dislocation arrangement and surface profile

Figure 3(a) shows an example of the dislocations distributed according to our model and the surface displacement caused by these dislocations. The positions of the dislocations are marked by vertical bars. Blue and green bars correspond to dislocations with opposite signs of the tilt component of the Burgers vector b_z. The large standard deviation of the distribution gives rise to bunches of dislocations separated by dislocation-free regions. The black curve in Fig. 3(a) denotes the surface displacement calculated for this dislocation array. On a mesoscopic scale, the surface relief exhibits rather sharp peaks caused by dislocation bundles separated by relatively flat regions. In calculating surface displacements from dislocations, we assume that the slip steps are eliminated by surface diffusion, as proposed by Andrews *et al.*,[23–25] so that the surface displacement due to each dislocation is a continuous function of the coordinate x. This choice is discussed in Sec. IV. The x-ray diffraction profile, calculated for this distribution of the dislocation positions, is shown in Fig. 3(d) by the black line. It is calculated at $q_z = q_{0z}$, i.e., at the q_z position in between the ones presented in Fig. 2(a), for the same model of the dislocation distribution.

Figures 3(b) and 3(c) present, for a comparison, more homogeneous dislocation distributions modeled in the literature.[23–25] The dislocation positions in Fig. 3(b) are chosen at random independently from each other, and the signs of the tilt components of their Burgers vectors are also not correlated. The dislocation density is the same, $\rho d = 0.5$. The surface displacements (red line) are qualitatively similar to those in Fig. 3(a) but have less pronounced peaks and smaller flat areas. However, the x-ray diffraction profile calculated for this model by the same Monte Carlo method [red curve in Fig. 3(d)] appears qualitatively different. It possesses the side maxima described theoretically for uncorrelated random misfit dislocations[16] and observed experimentally for $In_{0.1}Ga_{0.9}As$/GaAs(001),[15] $Si_{0.75}Ge_{0.25}$/Si(001),[16] and ZnSe/GaAs(001)[17,18] epitaxial films.

Figure 3(c) shows a model with random dislocation positions but correlated Burgers vectors. Alternating groups containing a given number of dislocations with the same tilt component of the Burgers vector b_z were considered in Ref. 25. In our model, the number of dislocations in a group is taken at random: the sign of b_z is changed with the probability $p = 0.1$ so that there are on average 10 dislocations in a group. The surface profile (blue line) varies over a larger lateral scale and a larger height. The diffraction profile calculated for this model [blue line in Fig. 3(e)] exhibits the same side maxima as the one for the case of uncorrelated positions and Burgers vectors above. Thus, the bunching of dislocations is required to explain our experimental diffraction profiles.

Figure 3(e) presents the surface relief of the investigated $Si_{0.4}Ge_{0.6}$/Si(001) film as measured by atomic force microscopy (AFM). The cross-hatch pattern observed in this micrograph is a well-known manifestation of plastic relaxation.[23–36] With the dislocation density $\rho d = 0.5$ as determined from the x-ray data, the number of dislocations on a 10 μm interval is 185, while only about 35 randomly spaced parallel lines are seen in Fig. 3(e). Hence, a single line in the AFM image corresponds to a group of dislocations rather than a single dislocation. This is in a good agreement with our analysis and the calculated profile in Fig. 3(a). Further discussion on the cross-hatch patterns is given in Sec. IV.

The expected shift q_{0z} of the coherent 004 peak due to an average strain calculated by the expression given above for the dislocation density of our sample ($\rho d = 0.5$) is equal to $q_{0z}d \approx 4.4$. This shift is taken into account in Fig. 2(b) so that the intensity maximum is expected to be at the origin, $q_z - q_{0z} = 0$. We have verified this prediction by additional Monte Carlo calculations (not shown) of similar diffraction profiles for uncorrelated or more ordered dislocations, which give the intensity maxima at the expected position. However, the peak of the calculated curve in Fig. 2(b) is at $(q_z - q_{0z})d \approx -2.65$. Hence, the coherent peak position corresponds to less than half of the actual film relaxation.

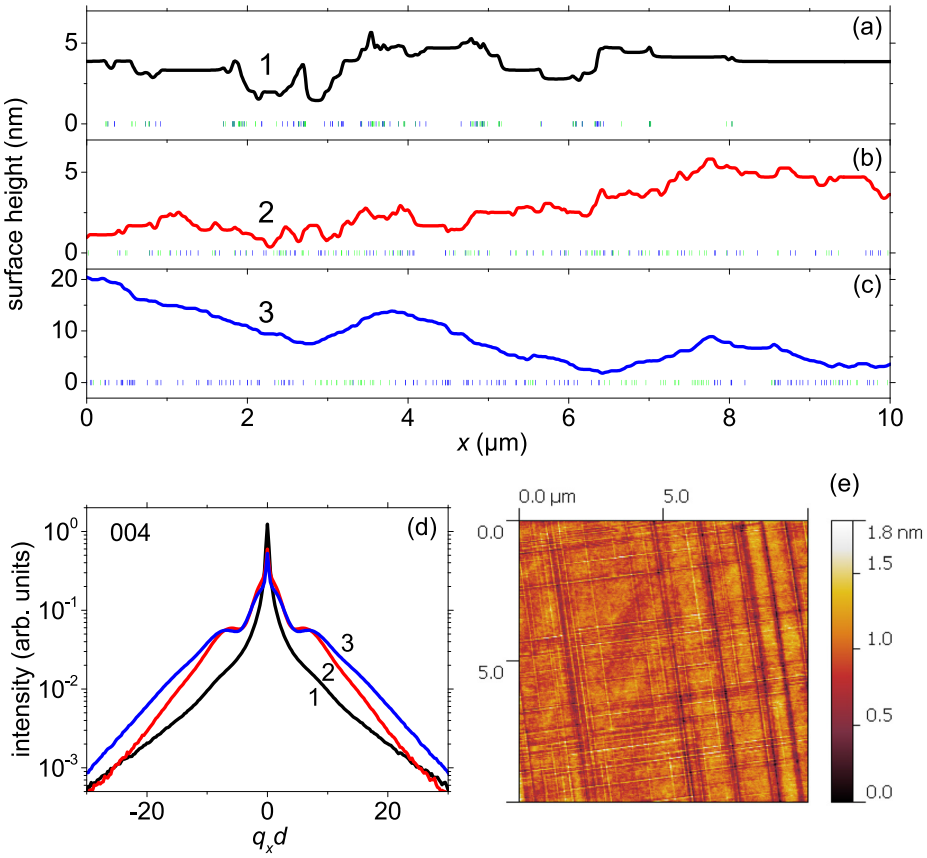

FIG. 3. [(a)–(c)] Examples of dislocation positions and surface profiles for different models of the dislocation arrangements. Blue and green bars represent dislocations with two different tilt components $\pm b_z$ of the Burgers vectors of 60° dislocations. (a) The model reproducing the experimental maps and profiles in Figs. 1 and 2: log-normal distribution of the dislocation positions with the standard deviation 10 times larger than the average distance between dislocations, random uncorrelated Burgers vectors. (b) Both positions and Burgers vectors are uncorrelated. (c) Uncorrelated dislocation positions and groups of dislocations with the same Burgers vectors, 10 dislocations in a group on average. (d) Diffraction profiles in symmetric reflection 004 for the three models in (a)–(c). (e) Atomic force microscopy image of the experimental sample showing the cross-hatch pattern.

The difference between expected and calculated peak positions can be explained by the dislocation bunching, which gives rise to regions with large and small strains, as it is reflected in the surface profile in Fig. 3(a). The dislocation-rich regions possess large strain and large strain inhomogeneity so that they contribute mostly to the diffuse scattering. In contrast, the dislocation-depleted regions possessing small strain and small strain gradients contribute to the coherent intensity. As a result, the positions of the coherent and the diffuse intensity maxima on the calculated reciprocal space maps in Figs. 1(e)–1(h) do not coincide: the coherent peak reflects the areas in the sample which are less strained than the average, while the diffuse peak represents the more strained ones.

The coherent peaks in Figs. 1(f)–1(h) remain at the same lateral position $q_x = 0$ as they are in an elastically relaxed dislocation-free film. This peak position has been analyzed in Ref. 16 [see discussion after Eq. (27)] and in Ref. 37. One can also see from the experimental maps in the insets in Figs. 1(a)–1(d) that the q_x-positions of the substrate and the film peaks coincide. The intensity maxima move to $q_x = q_{0x}$ when the dislocation density is increased, the coherent peak becomes weak, and the diffuse peak dominates.

IV. DISCUSSION

The $Si_{0.4}Ge_{0.6}$/Si film of thickness 27 nm studied in the present work is one of the thickness series grown at 450 °C. The films of the thicknesses up to 24 nm are dislocation free and possess the rms surface roughness below 0.1 nm. The low growth temperature suppresses surface diffusion and allows us to avoid elastic relaxation by surface roughening in the Stranski–Krastanov growth mode, which takes place at higher growth temperatures.

Plastic relaxation quickly develops after its onset: the relaxation of a 50 nm thick film of the same series is already $R = 0.6$ and increases further for thicker films. The analysis of the reciprocal space maps of these samples[12] shows that the positions of dislocations are not correlated, and the correlation parameter γ (defined in Ref. 16) is found to be close to 1. Hence, dislocations are introduced in the regions between bunches and make the dislocation distribution more homogeneous. However, the dislocations are still much less ordered than typically observed in other systems, where the correlation parameter γ occurs much smaller than 1.[16,38–40] Less correlated dislocation distribution in the present case can also be a consequence of the low growth temperature.

The cross-hatch patterns in semiconductor films were observed by x-ray topography already 45 years ago.[26,27] At the very early stages of relaxation, x-ray topography allows us to reveal almost each dislocation. The bunching of dislocations can be detected already at this stage by a difference between diffractometric and topographic measurements of the relaxation.[29] In the $Al_xGa_{1-x}As$/GaAs system studied in Ref. 29, dislocations along two orthogonal ⟨110⟩ directions possess different formation energies and a difference in relaxation between these two directions is seen. In the $Si_{1-x}Ge_x$/Si system studied in the present work, the ⟨110⟩ directions are equivalent and the relaxation is the same in both directions.

The cross-hatch patterns have been studied by the surface height measurements in many works.[23–25,27,28,30–36] In

one of the first papers on this topic, Hsu *et al.*[30] proposed that "the cross-hatch patterns arise from the inhomogeneous strain fields associated with the misfit dislocation combined with the long surface atom diffusion length at high growth temperatures". This general statement is supported in the subsequent works cited above, but already the number of these publications shows that a detailed description of the relaxation process and the formation of the cross-hatch pattern remain controversial.

A misfit dislocation gliding from the surface to the film—substrate interface leaves a slip step of the atomic height at the surface. The step either remains or is eliminated by surface diffusion.[23–25,32] We model the surface profiles in Fig. 3, accepting the latter possibility. From the standpoint of mathematical description of the dislocation displacement field, it means such a choice of the cut direction of the function $\arctan(z/x)$ that the displacement is continuous at the surface. Physically, it means that the surface diffusion is sufficient to provide the step motion so that the opposite steps due to dislocations with opposite tilt components of the Burgers vectors meet and compensate each other. This process involves much less surface diffusion than in the Stranski–Krastanov growth case, where surface diffusion gives rise to the surface height undulations which in turn cause generation of misfit dislocations (see, e.g., Ref. 41 and references therein). As we have already mentioned above, the low surface temperature allows us to avoid the Stranski–Krastanov growth.

When the thicknesses of the $Si_{0.4}Ge_{0.6}$ films in our thickness series are increased after the onset of plastic relaxation, the cross-hatch patterns evolve to larger rms surface roughness with more homogeneous distribution of roughness without flat regions, similarly to the transition from the profile in Fig. 3(a) to that in Fig. 3(b), which corresponds to a more homogeneous distribution of misfit dislocations which follows also from the x-ray diffraction patterns.[12]

The wings of diffuse scattering in Fig. 2(a) are provided by the tilt components of the 60° dislocations. Modeling of the Lomer (edge) misfit dislocations gives rise to qualitatively different profiles that cannot explain the x-ray diffraction data. It has been found recently[20,21] that a 60° misfit dislocation acts as a strain concentrator that can cause nucleation of a complimentary 60° dislocation. Dislocations in such a pair are separated by several nanometers and possess opposite tilt components of their Burgers vectors. The total strain field that they produce on distances larger than its separation is that of a Lomer dislocation so that such a pair is not distinguished in the x-ray diffraction experiment from a single Lomer dislocation.

V. SUMMARY

Diffuse x-ray intensity from misfit dislocations can be revealed at the very early stages of relaxation of the epitaxial films, when the shift of diffraction peaks due to these dislocations is not yet visible. The diffuse intensity distribution is sensitive to the spatial arrangement of misfit dislocations. We model the dislocation distribution by the Monte Carlo method and find that the diffraction pattern from a $Si_{0.4}Ge_{0.6}/Si(001)$ epitaxial film on the onset of relaxation is due to a very inhomogeneous dislocation distribution. Distances between dislocations vary very broadly so that the standard deviation of the dislocation spacings is 10 times larger than the mean distance between dislocations. In other words, dislocations form bunches, as a result of the action of the small number of dislocation sources. These bunches are seen as cross-hatch patterns in the AFM images of the film.

The inhomogeneous dislocation distribution results in peculiar features of the diffraction patterns. The positions of the coherent and the diffuse peaks do not coincide since the former is mostly due to undisturbed regions between dislocation bunches, while the latter is due to the inhomogeneous strain at the bunches. Moreover, since the coherent peak represents the undisturbed regions rather than the strain averaged over the whole film, its position at the onset of relaxation does not correspond to the actual density of misfit dislocations and underestimates relaxation by more than a factor of 2.

ACKNOWLEDGMENTS

The authors thank Bernd Jenichen and Oliver Brandt for a critical reading of the manuscript.

[1]*Silicon Heterostructure Handbook*, edited by J. D. Cressler (CRC Press, Boca Raton, 2006).
[2]E. A. Fitzgerald, Mater. Sci. Rep. **7**, 87 (1991).
[3]R. Hull and J. C. Bean, Crit. Rev. Solid State Mater. Sci. **17**, 507 (1992).
[4]S. C. Jain, A. H. Harker, and R. A. Cowley, Philos. Mag. A **75**, 1461 (1997).
[5]Yu. B. Bolkhovityanov, O. P. Pchelyakov, and S. I. Chikichev, Phys.-Usp. **44**, 655 (2001).
[6]K. Brunner, Rep. Prog. Phys. **65**, 27 (2002).
[7]M. Myronov, C. Morrison, J. Halpin, S. Rhead, C. Casteleiro, J. Foronda, V. A. Shah, and D. Leadley, Jpn. J. Appl. Phys., Part 1 **53**, 04EH02 (2014).
[8]H. Heinke, M. O. Möller, D. Hommel, and G. Landwehr, J. Cryst. Growth **135**, 41 (1994).
[9]D. K. Bowen and B. K. Tanner, *X-Ray Metrology in Semiconductor Manufacturing* (CRC Press, Boca Raton, 2006).
[10]A. Benediktovich, I. Feranchuk, and A. Ulyanenkov, *Theoretical Concepts of X-Ray Nanoscale Analysis* (Springer, Heidelberg, 2014).
[11]J. M. Hartmann, A. Abbadie, and S. Favier, J. Appl. Phys. **110**, 083529 (2011).
[12]T. Ulyanenkova, M. Myronov, A. Benediktovich, A. Mikhalychev, J. Halpin, and A. Ulyanenkov, J. Appl. Cryst. **46**, 898 (2013).
[13]R. People and J. C. Bean, Appl. Phys. Lett. **47**, 322 (1985).
[14]R. People and J. C. Bean, Appl. Phys. Lett. **49**, 229 (1986).
[15]P. Kidd, P. F. Fewster, and N. L. Andrew, J. Phys. D: Appl. Phys. **28**, A133 (1995).
[16]V. M. Kaganer, R. Köhler, M. Schmidbauer, R. Opitz, and B. Jenichen, Phys. Rev. B **55**, 1793 (1997).
[17]G. Alexe, H. Heinke, M. Klude, V. Kaganer, and D. Hommel, Phys. Status Solidi B **229**, 193 (2002).
[18]G. Alexe, H. Heinke, L. Haase, D. Hommel, J. Schreiber, M. Albrecht, and H. P. Strunk, J. Appl. Phys. **97**, 103506 (2005).
[19]Yu. B. Bolkhovityanov and L. V. Sokolov, Semicond. Sci. Technol. **27**, 043001 (2012).
[20]Yu. B. Bolkhovityanov, A. S. Deryabin, A. K. Gutakovskii, and L. V. Sokolov, Acta Mater. **61**, 617 (2013).
[21]A. Marzegalli, M. Brunetto, M. Salvalaglio, F. Montalenti, G. Nicotra, M. Scuderi, C. Spinella, M. De Seta, and G. Capellini, Phys. Rev. B **88**, 165418 (2013).
[22]V. M. Kaganer and K. K. Sabelfeld, Phys. Rev. B **80**, 184105 (2009).
[23]A. M. Andrews, J. S. Speck, A. E. Romanov, M. Bobeth, and W. Pompe, Appl. Phys. Lett. **77**, 3740 (2000).

[24]A. M. Andrews, J. S. Speck, A. E. Romanov, M. Bobeth, and W. Pompe, J. Appl. Phys. **91**, 1933 (2002).
[25]A. M. Andrews, R. LeSar, M. A. Kerner, J. S. Speck, A. E. Romanov, A. L. Kolesnikova, M. Bobeth, and W. Pompe, J. Appl. Phys. **95**, 6032 (2004).
[26]S. Kishinô, M. Ogirima, and K. Kurata, J. Electrochem. Soc. **119**, 617 (1972).
[27]G. H. Olsen, J. Cryst. Growth **31**, 223 (1975).
[28]K. H. Chang, R. Gibala, D. Srolovitz, P. K. Bhattacharya, and J. F. Mansfield, J. Appl. Phys. **67**, 4093 (1990).
[29]B. K. Tanner, A. G. Turnbull, C. R. Stanley, A. H. Kean, and M. McElhinney, Appl. Phys. Lett. **59**, 2272 (1991).
[30]J. W. P. Hsu, E. A. Fitzgerald, Y. H. Xie, P. J. Silverman, and M. J. Cardillo, Appl. Phys. Lett. **61**, 1293 (1992).
[31]S. Yu. Shiryaev, F. Jensen, and J. W. Petersen, Appl. Phys. Lett. **64**, 3305 (1994).
[32]M. A. Lutz, R. M. Feenstra, F. K. LeGoues, P. M. Mooney, and J. O. Chu, Appl. Phys. Lett. **66**, 724 (1995).
[33]M. Albrecht, S. Christiansen, J. Michler, W. Dorsch, H. P. Strunk, P. O. Hansson, and E. Bauser, Appl. Phys. Lett. **67**, 1232 (1995).
[34]R. Beanland, M. Aindow, T. B. Joyce, P. Kidd, M. Lourenço, and P. J. Goodhew, J. Cryst. Growth **149**, 1 (1995).
[35]B. Gallas, J. M. Hartmann, I. Berbezier, M. Abdallah, J. Zhang, J. J. Harris, and B. A. Joyce, J. Cryst. Growth **201**, 547 (1999).
[36]S. Saha, D. T. Cassidy, and D. A. Thompson, J. Appl. Phys. **113**, 124301 (2013).
[37]A. Benediktovitch, F. Rinaldi, S. Menzel, K. Saito, T. Ulyanenkova, T. Baumbach, I. D. Feranchuk, and A. Ulyanenkov, Phys. Status Solidi A **208**, 2539 (2011).
[38]S. Daniš and V. Holý, Phys. Rev. B **73**, 014102 (2006).
[39]A. Shalimov, J. Bak-Misiuk, V. M. Kaganer, M. Calamiotou, and A. Georgakilas, J. Appl. Phys. **101**, 013517 (2007).
[40]A. Benediktovitch, A. Zhylik, T. Ulyanenkova, M. Myronov, and A. Ulyanenkov, J. Appl. Cryst. **48**, 655 (2015).
[41]F. Rovaris, R. Bergamaschini, and F. Montalenti, Phys. Rev. B **94**, 205304 (2016).